Combustion and Flame 161 (2014) 2614–2626

Contents lists available at ScienceDirect

Combustion and Flame

journal homepage: www.elsevier.com/locate/combustflame

Influence of edge velocity on flame front position and displacement speed in turbulent premixed combustion

Sina Kheirkhah *, Ömer L. Gülder

University of Toronto Institute for Aerospace Studies, Toronto, Ontario M3H 5T6, Canada

ARTICLE INFO

Article history:
Received 3 October 2013
Received in revised form 10 January 2014
Accepted 13 April 2014
Available online 14 May 2014

Keywords:
V-shaped flame
Edge velocity
Flame front position
Flame displacement speed

ABSTRACT

Using a novel concept, the present study experimentally investigates underlying physics pertaining to statistics of the flame front position and the flame front velocity in turbulent premixed V-shaped flames. The concept is associated with characteristics of the reactants velocity at the vicinity of the flame front, referred to as the edge velocity. The experiments are performed using simultaneous Mie scattering and Particle Image Velocimetry techniques. Three mean streamwise exit velocities of: 4.0, 6.2, and 8.6 m/s along with three fuel–air equivalence ratios of: 0.7, 0.8, and 0.9 are examined. The results show that fluctuations of the flame front position and the flame front velocity are induced by the fluctuations of the component of the edge velocity transverse to the mean flow direction. Analysis of the results show that the mean of the flame front velocity in the normal direction to the flame front is significantly dependent on the vertical distance from the flame-holder. Relatively close to the flame-holder, the mean of the flame front velocity in the direction normal to the flame front is about zero; however, it increases to values several times larger than the laminar flame speed by increasing the vertical distance from the flame-holder.

1. Introduction

Turbulent premixed combustion is the mode of operation in several combustion equipment associated with electric-power generation and automotive industries, e.g., stationary gas turbines and spark ignition engines, respectively [1–3]. During the past decades, numerous laboratory settings have been developed to study characteristics of turbulent premixed flames; see, for example, review papers by Clavin [3], Lipatnikov and Chomiak [4], and Driscoll [5]. The flame configuration utilized in the present investigation is V-shaped. This study is motivated by the desire to investigate the underlying physics associated with the causality correlations between the governing parameters and the root-mean-square (RMS) of the flame front position (x') as well as the statistics of the flame front velocity ($\overrightarrow{V_f}$). Past studies [4,6,7] as well as a recent publication by the authors [8] show that, for lean conditions, x' increases by increasing the fuel–air equivalence ratio (ϕ). To the best knowledge of the authors, the underlying physics associated with this observation is yet to be investigated in detail. For the statistics of the flame front velocity, a survey of literature shows that the component of the flame front velocity in the direction normal to the flame front is correlated with the flame displacement speed (S_d) [5]. To the best knowledge of the authors, no experimental study has been performed to investigate this correlation in V-shaped flame configuration. The following provides a review of the literature associated with the RMS of the flame front position and the correlation between the component of the flame front velocity normal to the flame front and the flame displacement speed.

Several studies have investigated the RMS of the flame front position in turbulent premixed V-shaped flames; see, for example [4,6–8]. These studies show that x' is significantly dependent on the vertical distance from the flame-holder (y) as well as the turbulence intensity (u'/U), where U and u' are the mean and RMS of the velocity measured at the exit of the burner. Results presented in Lipatnikov and Chomiak [4] show that x' can be obtained from the following equations:

$$x' \approx yu'/U, \tag{1a}$$

$$x' \approx \sqrt{2y(u'/U)\Lambda}, \tag{1b}$$

where Λ is the integral length scale. As argued by Lipatnikov and Chomiak [4], application of either of the above equations depends on the value of the vertical distance from the flame-holder. Specifically, for relatively small and large vertical distances from the flame-holder, Eq. (1a) and (1b) can be utilized to estimate the RMS of the flame front position, respectively. The results presented in Eq. (1b) show that the RMS of the flame front position is

* Corresponding author.
E-mail address: kheirkhah@utias.utoronto.ca (S. Kheirkhah).

http://dx.doi.org/10.1016/j.combustflame.2014.04.008
0010-2180/

independent of the chemical characteristics of the fuel–air mixture, e.g., fuel–air equivalence ratio (ϕ). This is in contrast with the experimental results presented in [6–8]. In fact, the results of these studies show that, for relatively large vertical distances from the flame-holder, the RMS of the flame front position, in addition to y and the turbulence intensity, depends on the fuel–air equivalence ratio. Lipatnikov and Chomiak [4] argue that the controversy between the predictions of Eq. (1b) and the experimental results is due to incapability of the turbulent diffusion theory for predicting the effect of ϕ on the flame front dynamics [4].

The flame displacement speed (S_d) is the relative velocity of the propagation of the flame front with respect to the reactants flow in the direction normal to the flame front [5]. Correlation between the flame displacement speed and the flame front velocity is given by the following equation [5]:

$$S_d = (\overrightarrow{V_f} - \overrightarrow{V_e}) \cdot \vec{n}, \quad (2)$$

where $\overrightarrow{V_e}$ and $\vec{n}$ are the velocity of the reactants measured at the vicinity of the flame front and the unit vector normal to the flame front, respectively. In Eq. (2), the symbol $(\cdot)$ represents the inner product operation. Both experimental investigations [9,10] as well as direct-numerical-simulation (DNS) studies [11,12] associated with relatively small and moderate values of turbulence intensity show that the mean flame displacement speed is close to the laminar flame speed. In a recent study performed by Kerl et al. [10], it was shown that the flame displacement speed can vary from about $-0.4S_L$ to $4.5S_L$, with $\overline{S_d}$ being approximately $1.1S_L$.

In several experimental investigations [4,6–8], it has been established that, for lean conditions, the RMS of the flame front position increases with increasing the fuel–air equivalence ratio. The first objective of the present study is to investigate the underlying physical mechanisms associated with this phenomenon. The second objective is associated with studying the details of the correlation provided in Eq. (2) for turbulent premixed V-shaped flame configuration. Both objectives are pursued using a novel concept, referred to as the edge velocity. It is shown that the edge velocity can provide significant insight into current understanding of turbulent premixed combustion in V-shaped flames.

2. Experimental methodology

This section consists of the experimental setup utilized to produce the V-shaped flames, measurement techniques, and the experimental conditions tested.

2.1. Experimental setup

The V-shaped flames were generated using the burner shown in Fig. 1(a). The burner is composed of an expansion section, a settling chamber, a contraction section, and a nozzle. Details associated with the burner setup are provided in Kheirkhah and Gülder [8]. A flame-holder is placed close to the exit of the nozzle, see Fig. 1(a) and (b). The flame-holder is made of brass. It is cylindrical in shape and has a diameter (d) of 2 mm. The flame-holder is fixed with a flame-holder support (see Fig. 1(b)). Parallel and circular guiding holes were generated on the flame-holder support. The guiding holes serve as a sliding mechanism which allows for adjusting the distance between the flame-holder centerline and the exit plane of the burner (see Fig. 1(b)). This distance was fixed at 4 mm for all the experimental conditions of this study.

Two coordinate systems are utilized: the Cartesian coordinate system and a coordinate system with axes locally normal and tangent to the flame front. The details of the Cartesian coordinate system are presented here. Since the coordinate system with axes locally normal and tangent to the flame front is dependent on the flame front geometry, details associated with this coordinate system is presented in the results section. The Cartesian coordinate system overlaid on the flame-holder is shown in Fig. 1(b). Center of the coordinate system is located equidistant from both ends of the flame-holder and 5 mm above the burner exit plane. The y-axis of the coordinate system is normal to the exit plane of the burner. The x-axis is normal to both y-axis and the flame-holder centerline. The z-axis is normal to both x and y axes and lies along the span of the flame-holder.

A stainless steel perforated plate, with technical drawing presented in Fig. 2(a), was utilized for turbulence generation purposes. The plate has an outer diameter (D) of 48.4 mm and a thickness of 1 mm. Sixty-seven circular holes were generated on the plate. The holes are arranged in a hexagonal pattern. Each hole has a diameter (D_h) of 3.9 mm. The distance between two neighboring holes (s) is 5.7 mm. This arrangement of holes results in a plate blockage ratio of 58%. The plate was located at 48.4 mm upstream of the nozzle exit plane, as shown in Fig. 2(b).

2.2. Measurement techniques

As stated in the introduction section, one of the objectives of this study is to investigate the correlation provided in Eq. (2) for V-shaped flames. As can be seen from the equation, estimation of the reactants velocity at the vicinity of the flame front ($\overrightarrow{V_e}$) is of significant importance. This means that the flame front position as well as the reactants velocity data need to be acquired simultaneously. For this reason, simultaneous Mie scattering and Particle Image Velocimetry (PIV) techniques were utilized in the experiments. The Mie scattering data was used to estimate the flame front position; and the PIV data was used to estimate the velocity data at the vicinity of the flame front. The PIV technique is developed based on correlating two consecutive Mie scattering images. The first image of each PIV image-pair was used to obtain data associated with the flame front. Then, each image-pair was analyzed to obtain the corresponding velocity field data. This combination of Mie scattering and PIV techniques allowed for obtaining simultaneous data associated with the flame front position and the velocity at the vicinity of the flame front. The following provides details associated with the Mie scattering and the PIV techniques.

Mie scattering

Mie scattering is elastic scattering of light, with wave length λ, from particles, with average diameter d_p, when $d_p \gtrsim \lambda$ [13]. This technique has been used in the past studies [7,14,15] for investigating the flame front characteristics. An underlying assumption in application of the Mie scattering technique is that combustion occurs inside a relatively thin layer [8,16,17]. This assumption is referred to as the flamelet assumption [18]. Implication of the flamelet assumption is that if the reactants are seeded with particles which evaporate at the flame front, the light intensities scattered from the particles in the reactants region will be significantly larger than those in the products region. This marked difference in the light intensities is utilized for detection of the flame front [8,16,17,19]. Details associated with analysis of the Mie scattering images are provided in Kheirkhah and Gülder [8].

Particle Image Velocimetry

The Particle Image Velocimetry data is acquired for both reacting and non-reacting flow conditions. The PIV data associated with the reacting flow was used for studying the velocity at the vicinity of the flame front; and PIV data associated with the non-reacting flow experiments was used to evaluate the experimental conditions tested. Data related to the non-reacting flow experiments is provided in the experimental conditions section.

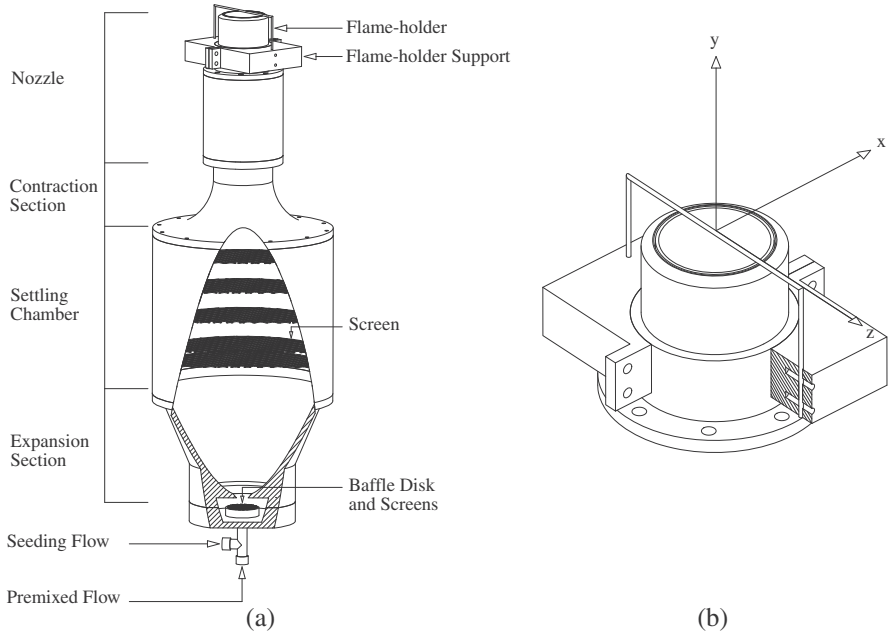

Fig. 1. (a) Burner setup and (b) flame-holder and flame-holder support details.

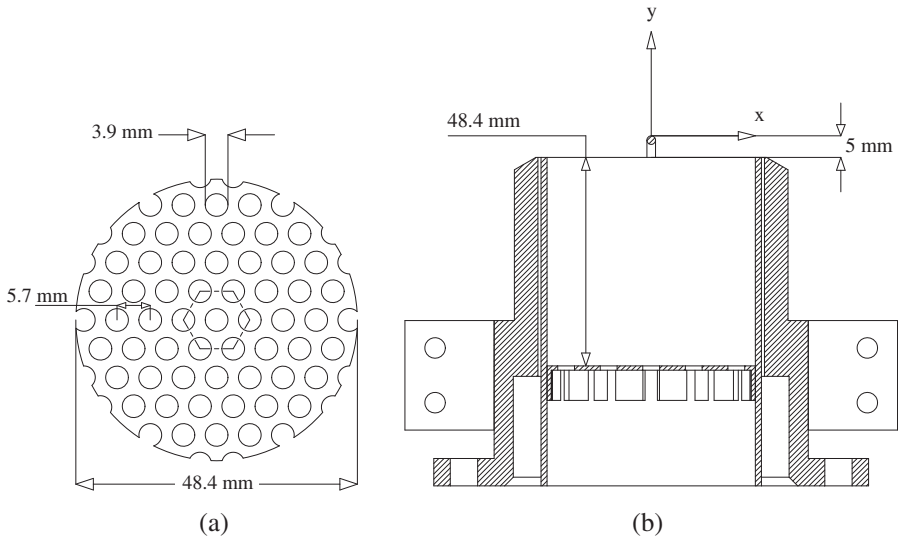

Fig. 2. (a) Perforated plate and (b) plate arrangement inside the burner nozzle.

The hardware associated with the PIV technique consists of a CCD camera and a Nd:YAG pulsed laser. The camera has a resolution of 2048 pixels by 2048 pixels. The camera head is equipped with a macro lens, which has a focal length (f) of 105 mm. During the experiments, the lens aperture size was fixed at $f/8$. The lens was equipped with a 532 nm band-pass filter. The filter was utilized in order to avoid influence of flame chemiluminescence in acquired images. For all the experiments, imaging field of view was approximately 60 mm × 60 mm.

The flow was illuminated by the laser. The laser produces a beam that is approximately 6.5 mm in diameter, which has a wavelength of 532 nm, energy of about 120 mJ per pulse, and a pulse duration of about 4 ns. All the experiments were performed at the plane of $z/d = 0$, where the laser sheet thickness is approximately 150 ± 50 μm. For statistical analysis, 1000 PIV image-pairs were acquired at a frequency of 5 Hz. For velocity data analysis, the interrogation box size was selected to be 16 pixels by 16 pixels, with zero overlap between the boxes. Olive oil droplets were used for seeding purposes in the PIV experiments. These droplets were previously assessed to be proper for the flow seeding. Details of the assessment are provided in Kheirkhah and Gülder [8].

2.3. Experimental conditions

The tested experimental conditions are tabulated in Table 1. Methane grade 2, i.e., methane with 99% chemical purity, was used as the fuel in the experiments. Three mean streamwise exit velocities of $U = 4.0$, 6.2, and 8.6 m/s were tested in the experiments. In Table 1, u' and v' are the RMS of the streamwise and transverse velocities estimated at $x/d = 0$, $y/d = -1$, and $z/d = 0$ for non-reacting flow condition and without the flame-holder. For each mean streamwise exit velocity, three fuel–air equivalence ratios of $\phi = 0.7$, 0.8, and 0.9 were tested. For each experimental condition, the integral length scale (Λ) was estimated from the

Table 1
Tested experimental conditions.

	Symbol	U^a	u'^a	v'^a	ϕ	$S_L{}^a$	$\delta_L{}^b$	η^b	Λ^b	Re_Λ	Ka	Da
Flame A	○	4.0	0.27	0.25	0.7	0.23	0.22	0.14	2.1	35.5	2.5	8.1
Flame B	□	4.0	0.27	0.25	0.8	0.30	0.17	0.14	2.1	35.5	1.5	13.7
Flame C	◇	4.0	0.27	0.25	0.9	0.37	0.14	0.14	2.1	35.5	1.0	20.6
Flame D	×	6.2	0.51	0.38	0.7	0.23	0.22	0.09	1.9	60.6	6.0	3.9
Flame E	+	6.2	0.51	0.38	0.8	0.30	0.17	0.09	1.9	60.6	3.6	6.6
Flame F	✻	6.2	0.51	0.38	0.9	0.37	0.14	0.09	1.9	60.6	2.4	9.8
Flame G	△	8.6	0.62	0.51	0.7	0.23	0.22	0.08	2.3	89.2	7.6	3.9
Flame H	◁	8.6	0.62	0.51	0.8	0.30	0.17	0.08	2.3	89.2	4.5	6.5
Flame I	▷	8.6	0.62	0.51	0.9	0.37	0.14	0.08	2.3	89.2	3.1	9.8

[a] The unit is in m/s.
[b] The unit is in mm.

autocorrelation of the streamwise velocity data [20] calculated along the y-axis. In Table 1, the laminar flame speed and the laminar flame thickness were obtained from the data provided by Andrews and Bradley [21] and Jarosinski [22], respectively. The Kolmogorov length scale (η) was obtained from $\eta = \Lambda Re_\Lambda^{-3/4}$. The Reynolds, Karlovitz, and Damköhler numbers are given by: $Re_\Lambda = u'\Lambda/\nu$, $Ka = (\delta_L/\eta)^2$, and $Da = S_L\Lambda/u'\delta_L$, respectively. The experimental conditions of the flames tested in the present investigation are overlaid on the premixed combustion regime diagram [1], as shown in Fig. 3. The experimental conditions correspond to the regimes of wrinkled flames, corrugated flames, and thin reaction zones.

3. Results

The results are associated with details pertaining to application of the velocity data measured at the vicinity of the flame front, referred to as the edge velocity ($\overrightarrow{V_e}$), in understanding of fundamental characteristics of V-shaped flames. The discussions are grouped into four sections. In Section 3.1., details of the algorithm utilized to estimate the edge velocity data are presented. In Sections 3.2., statistics of the streamwise and transverse components of the edge velocity data are studied. Then, underlying physics associated with these statistics and statistics of the flame front position are investigated in Section 3.3. In Section 3.4., the relation between the edge velocity, flame displacement speed, and flame front velocity are investigated.

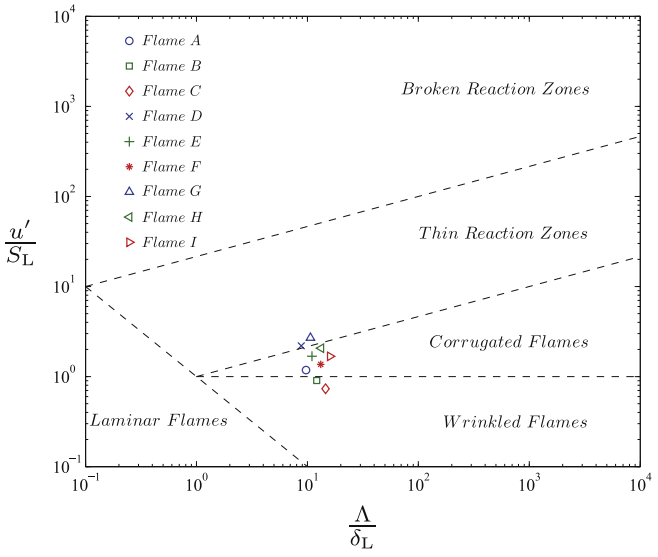

Fig. 3. Experimental conditions overlaid on the premixed combustion regime diagram [1].

3.1. Algorithm utilized for estimating the edge velocity

Details of the algorithm are presented below.

(I) A representative Mie scattering image associated with the experimental condition of Flame A is shown in Fig. 4(a). The flame fronts are presented by the highlighted curves on the figure. In order to demonstrate the concept of edge velocity, the region inside the white box in Fig. 4(a) is enlarged and presented in Fig. 4(b). The flame front in Fig. 4(b) is shown by the solid black curve. For a given normalized vertical distance from the flame-holder, e.g., $y/d = 22$, the corresponding point on the flame front, with similar value of y/d, was identified (see Fig. 4(b)). This point is labeled A in the figure.

(II) The tangent line at point A was obtained. This line is labeled L in Fig. 4(b).

(III) Centers of the interrogation boxes that enclose point A were identified. These points are labeled P_1, P_2, P_3, and P' in Fig. 4(b). An enlarged view of the region enclosed by these points is shown in Fig. 4(c).

(IV) From the points P_1, P_2, P_3, and P', those inside the reactants and products regions were identified. For the results presented in Fig. 4(c), P_1, P_2, and P_3 are located inside the reactants region, and P' is located inside the products region. From the points inside the reactants region, those with distances larger than 0.13 mm from the line L were selected. This distance is approximately equal to mean particle displacement between consecutive PIV images. Sensitivity analysis shows that this displacement causes inaccurate estimation of velocity data pertaining to the centers of the interrogation boxes located at distances from the line L smaller than the mean particle displacement. Thus, the velocity data estimated at the center of interrogation boxes with distances smaller than 0.13 mm from the line L were disregarded. For the results presented in Fig. 4(c), P_2 and P_3 are both located at distances from the line L that are larger than the mean particle displacement. These points were considered.

(V) From the centers of interrogation boxes considered in the previous step, the center with the least distance from the line L was selected. This point is labeled P_3 (see Fig. 4(c)). The velocity vector at point P_3 was considered. This velocity is referred to as the edge velocity ($\overrightarrow{V_e}$). The streamwise (u_e) and transverse (v_e) components of the edge velocity are shown in Fig. 4(c).

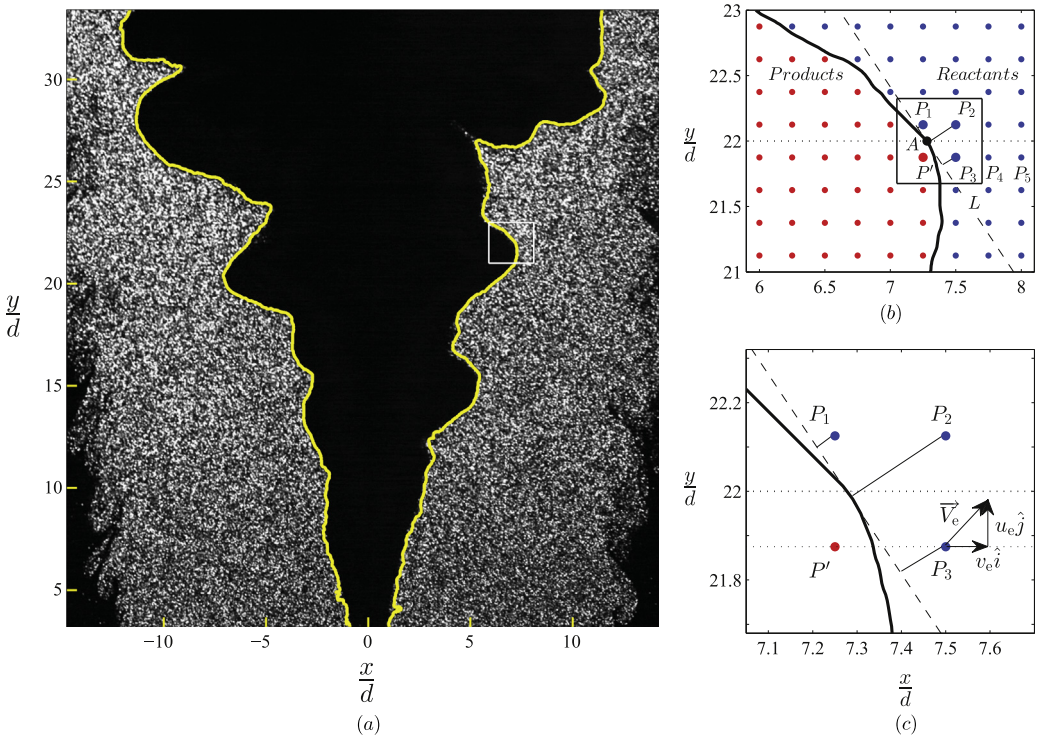

Fig. 4. (a) Representative Mie scattering image (b) flame front configuration, and (c) streamwise and transverse components of the edge velocity.

In the above algorithm, the distance between the flame front and the center of interrogation box (l) at which the edge velocity data is measured can potentially affect the statistics of the edge velocity data. For all experimental conditions tested and several vertical distances from the flame-holder, variation of $\bar{l}$ is presented in Fig. 5(a). As shown in the figure, $\bar{l}$ is on the order of the laminar flame thickness (see Table 1). In order to assess sensitivity of the edge velocity data to $\bar{l}$, the above algorithm was modified. The modification was performed in the last step of the algorithm. Specifically, after selecting the data at the center of the interrogation box that is positioned closest to the flame front, the edge velocity data was also selected at the centers of interrogation boxes that are spaced by one and two box width towards the reactants region (see points P_4 and P_5 in Fig. 4(b)). Then, mean streamwise ($\overline{u_e}$) and

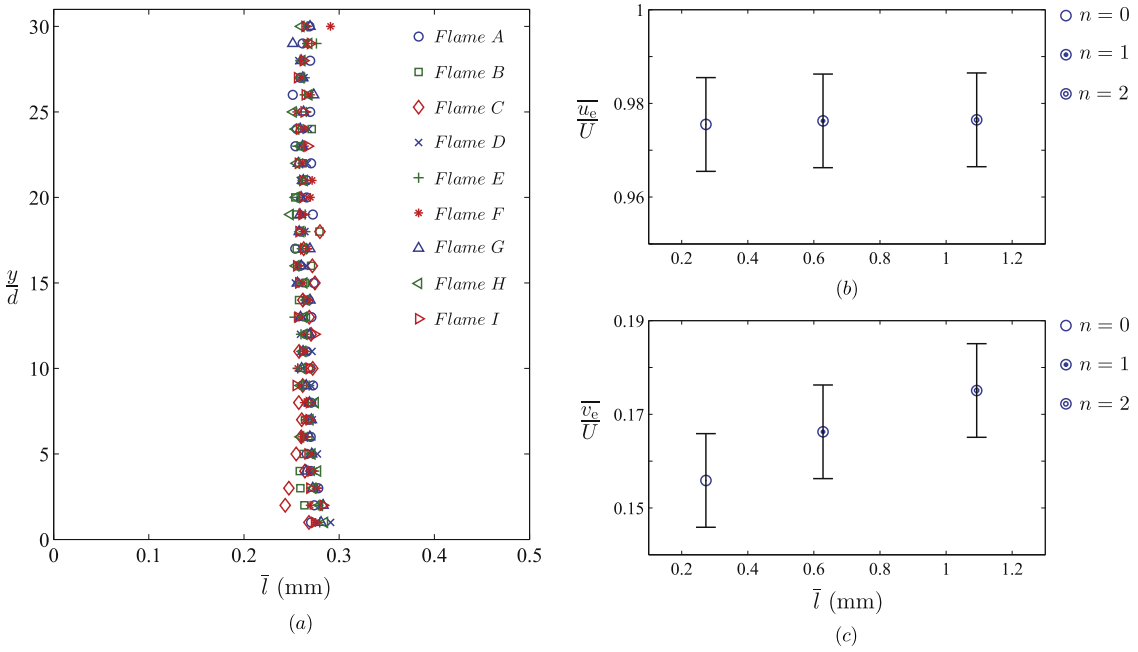

Fig. 5. (a) Variation of the mean of the distance between the flame front and the center of interrogation box at which the edge velocity data is selected. (b) and (c) correspond to mean streamwise and transverse components of edge velocity measured at center of interrogation boxes closest to the flame front ($n = 0$) as well centers spaced by one ($n = 1$) and two ($n = 2$) interrogation boxes towards the reactants region. The results in (b) and (c) correspond to Flame A condition and $y/d = 20$.

transverse ($\overline{v_e}$) edge velocities were estimated and presented in Fig. 5(b) and (c), respectively. The results in the figures correspond to the center of interrogation box positioned closest to the flame front ($n = 0$) and the points spaced by one ($n = 1$) and two ($n = 2$) interrogation box width towards the reactants region. These conditions are denoted by the number of interrogation box width spacing (n) in the figures data legends. The results in the figures pertain to normalized height above the flame-holder of $y/d = 20$. In Fig. 5(b) and (c), the error bars are associated with the uncertainties pertaining to estimation of the edge velocity data. As shown in Fig. 5(b), $\overline{u_e}$ does not vary by changing $\bar{l}$. However, the results in Fig. 5(c) show that increasing $\bar{l}$ by about 1 mm increases $\overline{v_e}/U$ by about 2%. This increase in $\overline{v_e}/U$ data is relatively small; and, as a result, it can be said that the statistics of the edge velocity data is not expected to vary significantly over distances from the flame front smaller than 1 mm.

3.2. Statistics of the edge velocity

Effects of the governing parameters on the mean and RMS of the edge velocity are presented in Figs. 6 and 7, respectively. Mean of the streamwise ($\overline{u_e}$) and transverse ($\overline{v_e}$) components of the edge velocity are presented in Fig. 6(a)–(c) and (d)–(f), respectively. The data symbols in Fig. 6(d)–(f) pertain to those in Fig. 6(a)–(c), respectively. The data in the first, second, and third columns corresponds to U = 4.0, 6.2, and 8.6 m/s, respectively. The uncertainties associated with the mean edge velocity data depend on the mean streamwise exit velocities and are almost independent of the fuel–air equivalence ratios tested. These uncertainties are accommodated by the sizes of the error bars shown in the corresponding figures. As presented in Fig. 6(a)–(c), the normalized mean streamwise edge velocity is dependent on the normalized vertical distance from the flame-holder. For all the experimental conditions tested, increasing the normalized vertical distance from the flame-holder increases $\overline{u_e}$. The results show that increasing the fuel–air equivalence ratio decreases $\overline{u_e}$ at small normalized vertical distances from the flame-holder ($y/d \lesssim 5$). At large normalized vertical distances from the flame-holder, with increasing U, the mean streamwise edge velocity becomes almost independent of the fuel–air equivalence ratio.

The normalized mean transverse edge velocity ($\overline{v_e}$) strongly depends on the fuel–air equivalence ratio. Results in Fig. 6(d)–(f) show that, for a fixed mean streamwise exit velocity and at a fixed vertical distance from the flame-holder, increasing the fuel–air equivalence ratio increases $\overline{v_e}$. This increase is speculated to be linked to the heat liberated at the flame front. Arguments provided in the past studies [14,23,24] indicate that the heat release directs the reactants towards the reactants region. Since, for the lean conditions tested, increasing ϕ increases the amount of heat release at the flame front, the reactants mass transfer towards the reactants region enhances with increasing the fuel–air equivalence ratio. Thus, it is expected that the normalized mean transverse edge velocity to increase with increasing the fuel–air equivalence ratio.

The results presented in Fig. 6 showed that, for a given mean bulk flow velocity and a fixed vertical distance from the flame-holder, increasing the fuel–air equivalence ratio decreases $\overline{u_e}$ and increases $\overline{v_e}$. The following arguments show that these trends can be explained for relatively small vertical distances from the flame-holder using a laminar flame model.

Comparison of the consecutive PIV images of the present study as well as analysis of the results of past investigations, e.g., Kheirkhah and Gülder [8] and Goix et al. [7] show that, relatively close to the flame-holder, the flame front is almost stationary. This means that $\overrightarrow{V_f} \approx \vec{0}$. Also, Mie scattering images of the present study show that, at small vertical distances from the flame-holder, the flame front is not disturbed by the turbulent flow. This observation along with the insignificant values of the flame front velocity ($\overrightarrow{V_f} \approx \vec{0}$) suggest that the state of the flame front is close to laminar at small vertical distances from the flame-holder. As a result, it was assumed that the flame displacement speed can be approximated by the laminar flame speed. This assumption along with $\overrightarrow{V_f} \approx \vec{0}$ were utilized to simplify Eq. (2) into:

$$S_L \approx -\overrightarrow{V_e} \cdot \vec{n}. \tag{3}$$

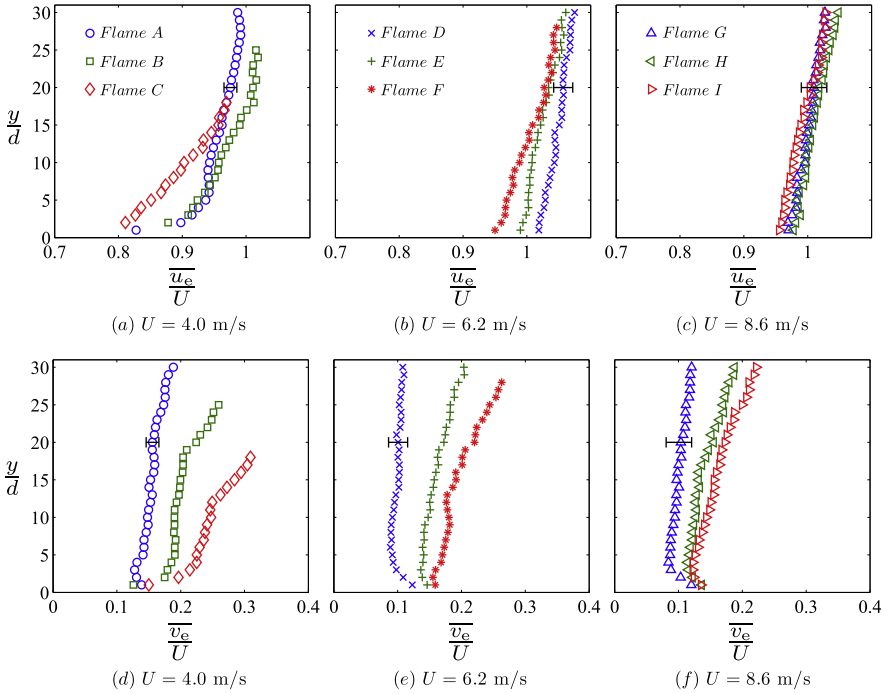

Fig. 6. (a)–(c) Normalized mean streamwise and (d)–(f) transverse components of edge velocity. The data symbols in (d)–(f) correspond to those in (a)–(c), respectively.

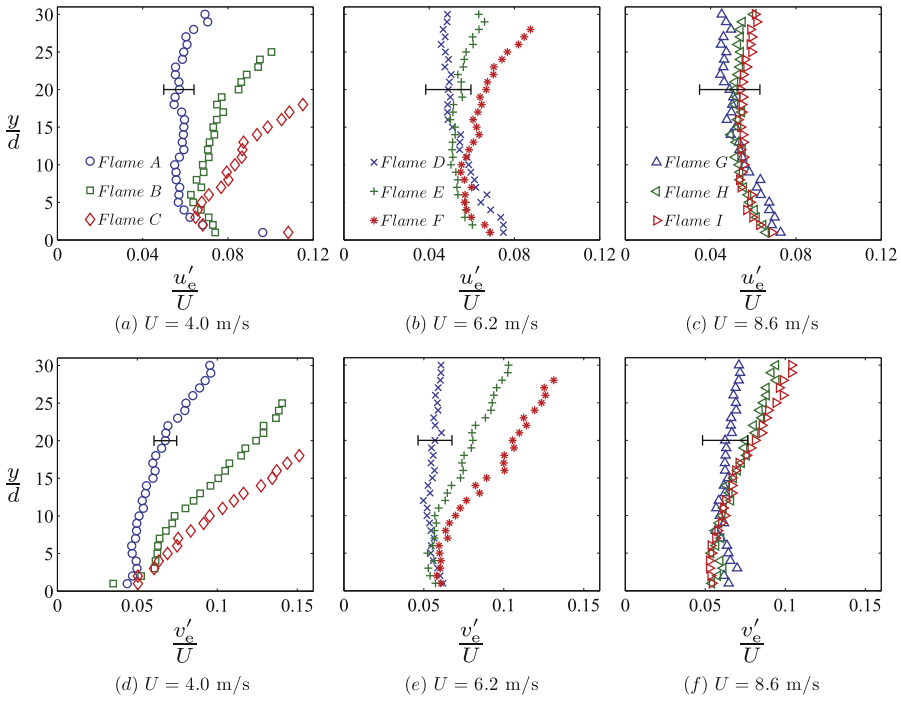

Fig. 7. (a)–(c) Normalized RMS of streamwise and (d)–(f) transverse components of edge velocity. The data symbols in (d)–(f) correspond to those in (a)–(c), respectively.

It can be shown that the normal vector to the flame front is given by: $\vec{n} = \sin(\theta)\hat{i} - \cos(\theta)\hat{j}$, where θ is the angle between tangent to the flame front and the horizontal axis. In the present study, θ was estimated following the methodology provided in Kheirkhah and Gülder [8]. Analysis of the results shows that for a fixed and small vertical distance from the flame-holder, θ is almost constant for all Mie scattering images associated with a given experimental condition. Values of $\tan(\theta)$ associated with $\phi = 0.7$ and for $y/d = 5$ are presented in Table 2. By time-averaging both sides of Eq. (3) and considering that $\overrightarrow{V_e} = v_e\hat{i} + u_e\hat{j}$, it is obtained that:

$$S_L \approx \overline{u_e}\cos(\theta) - \overline{v_e}\sin(\theta). \tag{4}$$

For a fixed vertical distance from the flame-holder and a fixed mean bulk flow velocity, both sides of Eq. (4) were differentiated with respect to the fuel–air equivalence ratio. Then, both sides of the equation were divided by $U\cos(\theta)$, resulting in:

$$\frac{1}{U\cos(\theta)}\frac{dS_L}{d\phi} \approx \frac{1}{U}\frac{d\overline{u_e}}{d\phi} - \frac{\overline{u_e}}{U}\frac{d\theta}{d\phi}\tan(\theta) - \frac{1}{U}\frac{d\overline{v_e}}{d\phi}\tan(\theta) - \frac{\overline{v_e}}{U}\frac{d\theta}{d\phi}. \tag{5}$$

In order to investigate the effect of ϕ on $\overline{u_e}$, as a first step approximation, it was assumed that $\overline{v_e} \approx 0$. Along with this assumption, the differentiations in Eq. (5) were approximated using the first order forward differencing scheme. These result in Eq. (5) simplifying to:

$$\frac{1}{U}\frac{\Delta\overline{u_e}}{\Delta\phi} \approx \frac{1}{U\cos(\theta)}\frac{\Delta S_L}{\Delta\phi} + \frac{\overline{u_e}}{U}\frac{\Delta\theta}{\Delta\phi}\tan(\theta). \tag{6}$$

The right-hand-side (RHS) of Eq. (6) can be utilized to study the effect of ϕ on the mean streamwise edge velocity for small normalized vertical distances from the flame-holder. Values of the first term on the RHS of Eq. (6) depend on the experimental conditions tested and the corresponding estimations are presented in Table 2. Experimentally obtained values of $\overline{u_e}/U$, at $y/d = 5$ and for Flames A, D, and G, were utilized for estimating the second term on the RHS of Eq. (6). The values are presented in Table 2 and are denoted by the *exp.* index. Also presented in the table are the values of $\Delta\overline{u_e}/U\Delta\phi$ obtained from the summation of the first and second terms on the RHS of Eq. (6) as well as the values obtained from the experimental results pertaining to $y/d = 5$. The experimentally estimated values of $\Delta\overline{u_e}/(U\Delta\phi)$ are denoted by the index of *exp.* in the table. As can be seen from the results in Table 2, the values associated with the model, in agreement with the experimental results, predict that $\overline{u_e}$ decreases with increasing the fuel–air equivalence ratio. However, the results in the table show that values of $\Delta\overline{u_e}/(U\Delta\phi)$ obtained from the mathematical model in Eq. (6) are significantly different from those estimated by the experimental results. This is speculated to be linked to the simplifying assumptions utilized for derivation of Eq. (6).

In order to investigate the effect of the fuel–air equivalence ratio on the mean transverse edge velocity, the following equation was utilized.

$$\frac{1}{U}\frac{\Delta\overline{v_e}}{\Delta\phi}\tan(\theta) \approx -\frac{1}{U\cos(\theta)}\frac{\Delta S_L}{\Delta\phi} + \frac{1}{U}\frac{\Delta\overline{u_e}}{\Delta\phi} - \frac{\overline{u_e}}{U}\frac{\Delta\theta}{\Delta\phi}\tan(\theta). \tag{7}$$

Eq. (7) was obtained from Eq. (5) using the following simplifications. First, the differentiations in Eq. (5) were estimated using the first order forward differencing scheme. Second, it was assumed that the last term on the RHS of Eq. (5) is significantly smaller than the second term on the RHS of the equation; and, as a result, the last

Table 2
Estimated values of the terms in Eqs. (6) and (7). The subscript exp. pertains to the experimentally estimated value of the corresponding term.

U(m/s)	$\tan(\theta)$	$\frac{1}{U\cos(\theta)}\frac{\Delta S_L}{\Delta\phi}$	$\frac{\overline{u_e}}{U}\frac{\Delta\theta}{\Delta\phi}\tan(\theta)\vert_{exp.}$	$\frac{\Delta\overline{u_e}}{U\Delta\phi}$	$\frac{\Delta\overline{u_e}}{U\Delta\phi}\vert_{exp.}$	$\frac{\Delta\overline{v_e}}{U\Delta\phi}\tan(\theta)$	$\frac{\Delta\overline{v_e}}{U\Delta\phi}\tan(\theta)\vert_{exp.}$
4.0	4.0	0.7	−2.6	−1.9	−0.6	1.3	1.7
6.2	6.2	0.7	−2.9	−2.2	−0.4	1.8	2.4
8.6	6.7	0.6	−1.8	−1.2	−0.1	1.1	1.7

term on the RHS of Eq. (5) was neglected. This is a valid assumption since the experimental results show that $\overline{u_e} > \overline{v_e}$ (see Fig. (6)) and $\tan(\theta) > 1$ (see Table 2). The values of $\Delta\overline{v_e}\tan(\theta)/(U\Delta\phi)$ were estimated using the RHS of Eq. (7) and presented in Table 2. For the first term on the RHS of Eq. (7), the results previously obtained and presented in Table 2 were utilized. For the second and third terms, the experimentally estimated values presented in the table were used. For comparison purposes, the experimentally estimated values of $\Delta\overline{v_e}\tan(\theta)/(U\Delta\phi)$ denoted by the *exp.* index, are also presented in Table 2. The results show that the values of $\Delta\overline{v_e}\tan(\theta)/(U\Delta\phi)$ obtained from the mathematical model in Eq. (7) are reasonably close to the corresponding experimentally obtained values. Also, the results of the mathematical model, in agreement with the experimental results, show that increasing ϕ increases $\overline{v_e}$.

Note that, due to relatively coarse resolution in variation of ϕ in the experimental conditions tested, the finite difference values provided in Table 2 are not expected to provide accurate estimations of the derivatives in Eq. (5). However, the estimations can be utilized to assess the trends associated with the effects of ϕ on the mean of the streamwise and transverse components of the edge velocity. In essence, the results of Eqs. (6) and (7) show that, for relatively small vertical distances from the flame-holder, the mathematical model presented in Eq. (5) can reasonably predict the trends present in Fig. 6.

Root-mean-square of streamwise (u'_e) and transverse (v'_e) components of the edge velocity are presented in Fig. 7(a)–(c) and (d)–(f), respectively. The data symbols in Fig. 7(d)–(f) correspond to those in Fig. 7(a)–(c), respectively. The data in the first, second, and third columns corresponds to U = 4.0, 6.2, and 8.6 m/s, respectively. The uncertainties pertaining to both u'_e and v'_e are accommodated by the sizes of the error bars in the corresponding figures. As shown in the figures, u'_e/U depends significantly on both y/d and the fuel–air equivalence ratio. For $y/d \lesssim 5$, u'_e/U decreases with increasing the normalized vertical distance from the flame-holder. However, for relatively large vertical distances from the flame-holder, increasing y/d increases u'_e/U. Effect of the fuel–air equivalence ratio is more pronounced at large vertical distances from the flame-holder. The results show that, for large vertical distances from the flame-holder, increasing ϕ increases u'_e/U. For example, for U = 4.0 m/s and at $y/d = 15$, increasing the fuel–air equivalence ratio from 0.7 to 0.9 increases u'_e/U by about 70%.

The results presented in Fig. 7(d)–(f) show that, with increasing the vertical distance from the flame-holder, RMS of the transverse edge velocity either remains almost constant (see Flames D and G), or increases (see all flame conditions except Flames D and G). Also, for a fixed mean streamwise exit velocity, increasing the fuel–air equivalence ratio increases the RMS of the transverse edge velocity. The trend of variations of v'_e with the vertical distance from the flame-holder, for all experimental conditions except Flame D and G, as well as the trend associated with the effect of ϕ on v'_e are of significant importance. This is because these trends are similar to the trends pertaining to the effect of ϕ and y on the RMS of the flame front position (x') reported in past investigations [4,8]. Details associated with these similarities and the corresponding physical implications are provided in the following section.

3.3. Edge velocity and flame front position

Kheirkhah and Gülder [8] investigated characteristics of the flame front position (x) for identical flame geometry and experimental conditions presented in this study. In their investigation [8], the flame front position is referred to as the distance between the flame front and the vertical axis (y). Variations of RMS of the flame front position (x') with vertical distance from the flame-holder and for all the experimental conditions tested are reproduced from Kheirkhah and Gülder [8] and are presented in Fig. 8. The results in Fig. 8(a)–(c) correspond to mean streamwise exit velocities of 4.0, 6.2, and 8.6 m/s, respectively. In the figures, the sizes of the error bars correspond to the uncertainties associated with estimation of x'. As shown in Fig. 8(a)–(c), for a fixed mean streamwise exit velocity, increasing the vertical distance from the flame-holder as well as the fuel–air equivalence ratio increase the RMS of the flame front position. These trends are similar to those of the RMS of the transverse edge velocity (see Fig. 7(d)–(f)). The similarities between the trends associated with the results in Figs. 7 and 8 suggest that the RMS of the flame front position can be potentially related to the RMS of the transverse edge velocity.

Using the results presented in Fig. 7 along with those presented in Fig. 8, variation of x'/d versus v'_e/U are presented in Fig. 9. Results in Fig. 9(a)–(c) correspond to mean streamwise exit velocities of $U = 4.0$, 6.2, and 8.6 m/s, respectively. As shown in Fig. 9(a)–(c), for a fixed mean streamwise exit velocity, increasing the RMS of the transverse edge velocity (v'_e) increases the RMS of the flame front position (x').

It was previously shown that increasing the fuel–air equivalence ratio increases RMS of the flame front position. For example, results presented in Fig. 8 show that, at a fixed mean streamwise exit velocity of $U = 4.0$ m/s and at $y/d = 15$, increasing ϕ from 0.7 to 0.9 increases x'/d from about 0.7 to 1.6. These two data points are highlighted by arrows in Fig. 8(a). Comparison of the experimental conditions associated with these data points indicate that, since the RMS of streamwise velocity at the exit of the burner (u') is fixed for Flames A and C, increasing the fuel–air equivalence ratio decreases u'/S_L. As a result, the effect of turbulence attenuates by increasing ϕ. This means that the RMS of the flame front position should decrease by increasing the fuel–air equivalence ratio. This conclusion is in contrast with the results presented in Fig. 8(a)–(c). In order to investigate this discrepancy, the data points corresponding to the arrows in Fig. 8(a) are highlighted in Fig. 9(a). As can be seen in Fig. 9(a), the values of the RMS of the normalized transverse edge velocity, corresponding to these data points, are about 0.06 and 0.12. This means that the increase in the fuel–air equivalence ratio results in a significant increase in the RMS of transverse edge velocity. Thus, it can be concluded that the reason for the increase of the RMS of the flame front position may be linked to the increase in the RMS of the fluctuations of the transverse component of the edge velocity. In fact, the results in Fig. 9 show that, at a fixed value of v'_e, increasing the fuel–air equivalence ratio decreases the RMS of the flame front position. This means that, for fixed turbulence conditions at the vicinity of the flame front, increasing the fuel–air equivalence ratio towards the stoichiometric condition ($\phi = 1$) increases the combustion stability; and, as a result, RMS of the flame front position decreases.

The arguments provided above show that fluctuations of the flame front position can be induced by the fluctuations of the transverse component of the reactants velocity at the vicinity of the flame front. It is speculated that the causality correlation between the transverse component of the edge velocity (v_e) and the flame front position (x) can be formed by the transverse component of the flame front velocity, referred to as v_f. Specifically, it is hypothesized that the fluctuations of the transverse component of the reactants velocity at the vicinity of the flame front induces fluctuations of the velocity of the flame front; and, as a result, position of the flame front changes. Thus, estimating the values of v'_f, and studying the correlations between this parameter and v'_e and x' are of significant importance in validating this hypothesis. Root-mean-square of the transverse component of the flame front velocity (v'_f) was estimated using the Taylor's theory of turbulent diffusion [25]. Arguments provided in Appendix A show that v'_f can be estimated from the following equation:

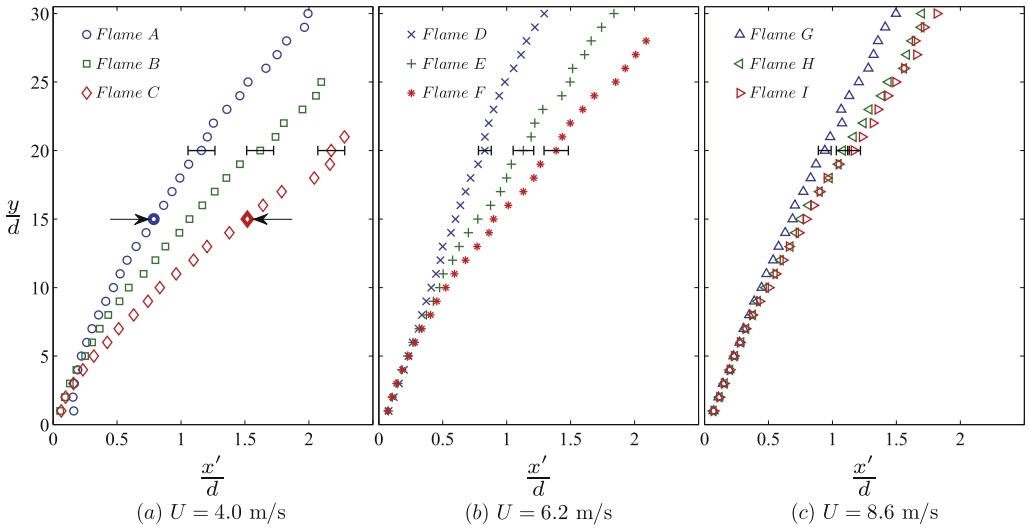

Fig. 8. Root-mean-square of the flame front position (x'). The data is reproduced from Kheirkhah and Gülder [8]. (a)–(c) correspond to $U = 4.0$, 6.2, and 8.6 m/s, respectively.

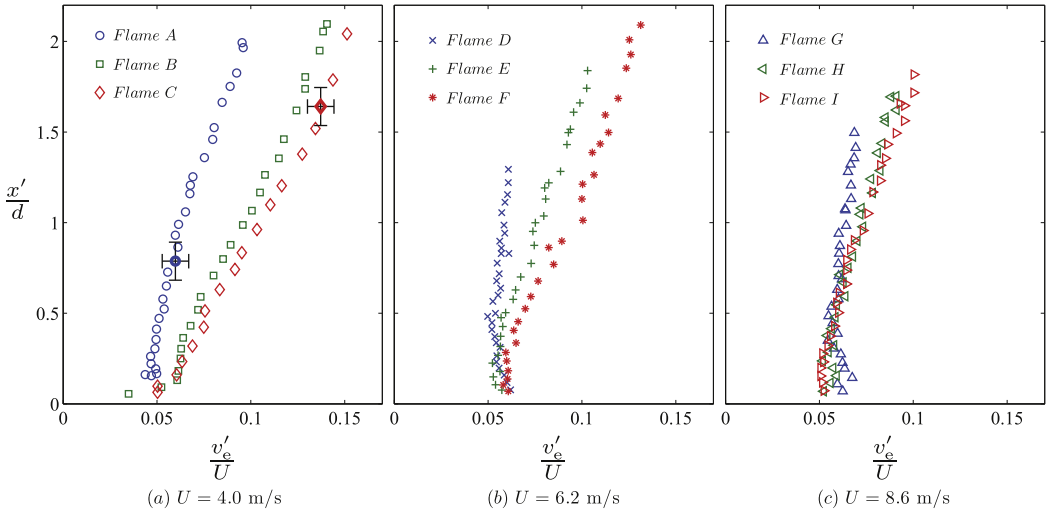

Fig. 9. Root-mean-square of flame front position and root-mean-square of transverse edge velocity. (a)–(c) correspond to $U = 4.0$, 6.2, and 8.6 m/s, respectively.

$$v'_f \approx x'U/y. \tag{8}$$

For all the experimental conditions tested, RMS of the transverse component of the flame front velocity was estimated using Eq. (8). The values of v'_f along with the corresponding values of v'_e are presented in Fig. 10. The error bars in the figure pertain to the uncertainty associated with estimating the values of v'_f and v'_e. Also overlaid on the figure is the dashed line pertaining to $v'_f = v'_e$. The results presented in the figure show that, for all the experimental conditions tested, increasing v'_e from about 0.2 m/s to 0.9 m/s increases v'_f from approximately 0.2 m/s to 0.6 m/s. This increase is such that the values of v'_f lie below the line of $v'_f = v'_e$. Also, the results in Fig. 10 show that the correlation between v'_f and v'_e is almost independent of the experimental conditions tested. This means that changing the experimental conditions, for example, the fuel–air equivalence ratio, changes RMS of the transverse component of the edge velocity, following the results presented in Fig. 9. The variation in v'_e leads to variation of the RMS of the transverse component of the flame front velocity. Then, v'_f causes fluctuations in position of the flame front, whose root-mean-square can be obtained from Eq. (A1), provided in Appendix A.

3.4. Relation between edge and flame front velocities

Results presented in previous section showed that the edge velocity plays a significant role in underlying physics associated with the dynamics of turbulent premixed V-shaped flames. Specifically, the correlation between the RMS of the transverse components of the edge velocity and flame front velocity were studied. In this section, the edge velocity concept is utilized to gain insight into the normal component of the flame front velocity. These two velocities are correlated by the flame displacement speed (S_d), given by Eq. (2). Time-averaging both sides of Eq. (2) and rearranging results in:

$$\overline{\vec{V_e} \cdot \vec{n}} = \overline{\vec{V_f} \cdot \vec{n}} - \overline{S_d}. \tag{9}$$

In order to estimate the term on the LHS of Eq. (9), the edge velocity data needs to be obtained in a coordinate system with axes locally perpendicular and tangent to the flame front. Configuration of a representative flame front is shown in Fig. 11, which is identical to that previously presented in Fig. 4(c). The edge velocity vector, $\vec{V_e}$, along with its components in the Cartesian coordinate system is presented in the figure. Also included in the figure are the axes

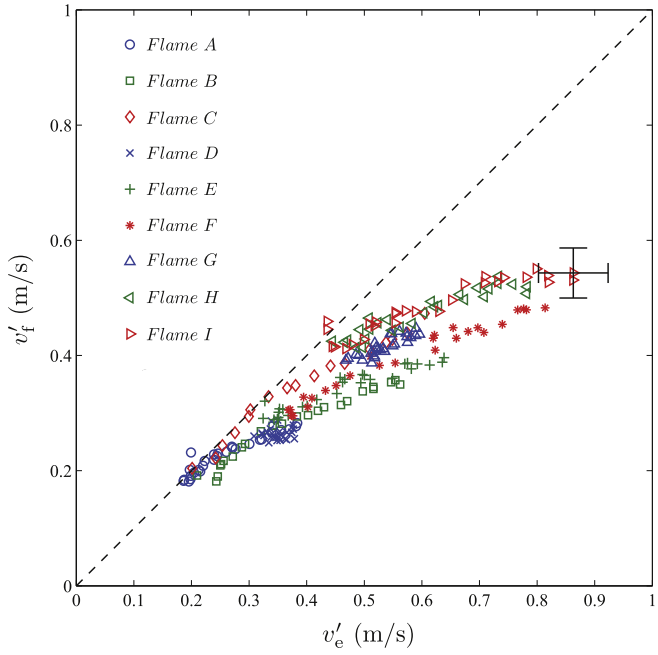

Fig. 10. RMS of the transverse component of the edge velocity and RMS of the transverse component of the flame front velocity. The dashed line corresponds to $v'_f = v'_e$.

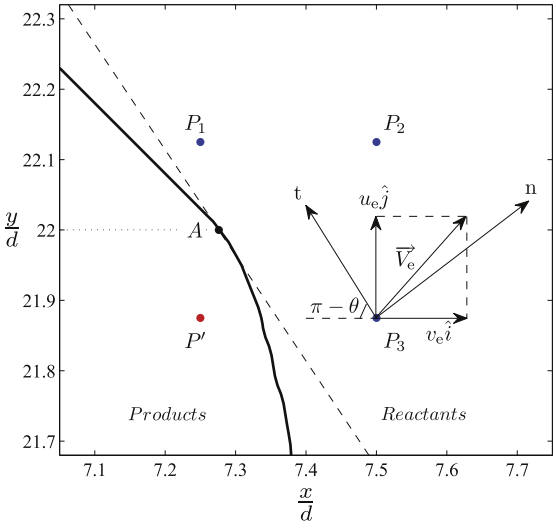

Fig. 11. Normal and tangent directions to the flame front.

normal (n) and tangent (t) to the flame front. From the configuration presented in Fig. 11, it can be shown that $\overrightarrow{V_e} \cdot \vec{n} = -u_e \cos(\theta) + v_e \sin(\theta)$; and, as a result:

$$\overline{\overrightarrow{V_e} \cdot \vec{n}} = \overline{-u_e \cos(\theta)} + \overline{v_e \sin(\theta)}, \tag{10}$$

where u_e and v_e are the streamwise and transverse components of the edge velocity vector ($\overrightarrow{V_e}$), with the corresponding characteristics presented in Section 3.2. Note that the formulation provided on the RHS of Eq. (10) is obtained based on two-dimensional measurements. An assessment associated with the effect of flow three-dimensionality on the LHS of Eq. (10) is provided in Appendix B.

Using Eq. (10), the mean of the normal component of the edge velocity was estimated for all experimental conditions tested, with the corresponding results presented in Fig. 12. The results presented in Fig. 12(a)–(c) correspond to mean streamwise exit velocities of $U = 4.0$, 6.2, and 8.6 m/s, respectively. For each experimental condition tested, $\overrightarrow{V_e} \cdot \vec{n}$ is normalized by the laminar flame speed (S_L) of the corresponding experimental condition. The uncertainty associated with mean of the normal component of the edge velocity is approximately ±23%. The results show that relatively close to the flame-holder ($y/d \lesssim 5$), $\overline{\overrightarrow{V_e} \cdot \vec{n}} \approx -S_L$. This can be explained by considering that the state of the flame front is almost laminar at small vertical distances from the flame-holder similar to the discussions presented in Section 3.2. Specifically, due to insignificant movements of the flame front, $\overrightarrow{V_f} \approx \vec{0}$; and, as a result, $\overline{\overrightarrow{V_f} \cdot \vec{n}} \approx 0$. Also, for small values of y/d, the mean flame displacement speed is approximately equal to the laminar flame speed. Thus, from Eq. (9), it is obtained that the mean of the normal component of the edge velocity is approximately equal to the negative of the laminar flame speed. This is in agreement with the results presented in Fig. 12, for relatively small vertical distances from the flame-holder.

For relatively large vertical distances from the flame-holder, movements of the flame front are significant; and, as a result, $\overrightarrow{V_f}$ is a nonzero vector. It can be mathematically shown that, for

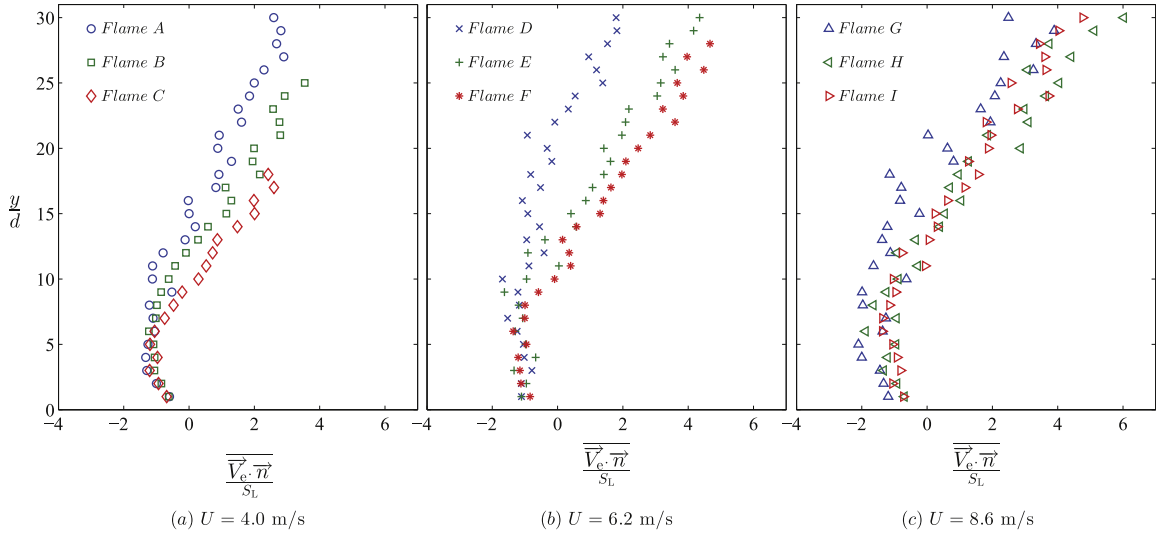

Fig. 12. Mean of the normal component of the edge velocity. (a)–(c) correspond to $U = 4.0$, 6.2, and 8.6 m/s, respectively.

confined flame configurations, the mean of the flame front velocity is a zero vector, i.e., $\overrightarrow{V_f} = \vec{0}$, with detailed proof provided in Appendix C. Although, for confined flames, the mean flame velocity is a zero vector, the mean of the component of the flame front velocity normal to the front ($\overrightarrow{V_f} \cdot \vec{n}$) is not necessarily zero. This is because the normal component of the flame front velocity is estimated in a non-stationary coordinate system. An example that proves $\overrightarrow{V_f} \cdot \vec{n}$ can be nonzero is presented in Appendix C. Results presented in Fig. 12 can be utilized to investigate mean of the normal component of the flame front velocity. In order to gain insight into characteristics of $\overrightarrow{V_f} \cdot \vec{n}$, the mean flame displacement speed has to be known. Although the statistics associated with the normal component of the flame front velocity as well as that of the edge velocity can be dependent on the flame configuration studied, the statistics of the flame displacement speed is independent of the flame configuration. This allows for utilizing the results from past investigations in order to gain further insight into the results in Fig. 12. In a recent study, using a three dimensional measurement technique, Kerl et al. [10] investigated the flame displacement speed for a premixed flame stabilized in a diffuser type burner. The results in Kerl et al. [10] show that mean of the flame displacement speed is close to the laminar flame speed ($\overline{S_d} \approx 1.1 S_L$). This means that, the mean of the normal component of flame front velocity can be given by:

$$\overrightarrow{V_f \cdot \vec{n}} \approx \overrightarrow{V_e} \cdot \vec{n} + 1.1 S_L. \tag{11}$$

For large vertical distances from the flame-holder, the results presented in Fig. 12 show that the mean of the normal component of the edge velocity can become several times larger than the laminar flame speed. Thus, considering that the mean flame displacement speed is on the order of the laminar flame speed, it can be concluded that the mean of the normal component of the flame front velocity is several times larger than the laminar flame speed at relatively large vertical distances from the flame-holder.

4. Concluding remarks

Characteristics of edge velocity, i.e., the reactants velocity at the vicinity of the flame front, was investigated experimentally. The edge velocity concept allowed for providing insight into physical mechanisms associated with the correlation between the governing parameters and characteristics of turbulent premixed V-shaped flames, specifically, the flame front position and the flame front velocity. Simultaneous Mie scattering and Particle Image Velocimetry techniques were utilized in the experiments. The Mie scattering data was used to obtain the flame front contour. The PIV experiments were performed to obtain the unburnt gas velocity at the vicinity of the flame front as well as to estimate the turbulent flow characteristics under non-reacting flow conditions. The experiments were performed for three mean streamwise exit velocities of: 4.0, 6.2, and 8.6 m/s along with three fuel–air equivalence ratios of: 0.7, 0.8, and 0.9.

Analysis of the results shows that there exists a causality correlation between the governing parameters and the RMS of the flame front position (x'). Specifically, it is hypothesized that changing the governing parameters changes the RMS of the transverse component of the edge velocity (v'_e). This causes a variation in the RMS of the transverse component of the flame front velocity (v'_f), which results in changing the RMS of the flame front position (x'). The RMS of the transverse component of the edge velocity (v'_e) was experimentally estimated, and RMS of the transverse component of the flame front velocity (v'_f) was estimated using the Taylor's theory of turbulent diffusion. The results show that the correlation between RMS of the transverse component of the edge velocity and the RMS of the transverse component of the flame front velocity is independent of the experimental conditions tested, suggesting that the correlation is a fundamental characteristic of turbulent premixed V-shaped flames.

Using the edge velocity concept, the mean of the flame front velocity in the normal direction to the flame front ($\overrightarrow{V_f} \cdot \vec{n}$) was estimated. The results show that relatively close to the flame-holder, and in agreement with the results of past investigations, $\overrightarrow{V_f} \cdot \vec{n} \approx 0$. Increasing the vertical distance from the flame flame-holder, increases $\overrightarrow{V_f} \cdot \vec{n}$ to values several times larger than the laminar flame speed.

Acknowledgments

The authors are grateful for financial support from the Natural Sciences and Engineering Research Council (NSERC) of Canada.

Appendix A. Estimation of root-mean-square of transverse component of the flame front velocity

The Taylor's theory of turbulent diffusion [25] was utilized to estimate the root-mean-square (RMS) of the transverse component of the flame front velocity (v'_f). Although the theory [25] was developed in order to study dispersion of particles in a turbulent flow, it can be utilized to analyze movements of turbulent premixed flames [4]. The turbulent diffusion theory indicates that the correlation between RMS of the flame front position and RMS of the transverse component of the flame front velocity can be obtained from the following equation:

$$x'^2 = 2 v'^2_f \int_0^{y/U} \int_0^t R_\xi \mathrm{d}\xi \mathrm{d}t, \tag{A1}$$

where t is time, and ξ is an arbitrary integration variable, with $0 \leqslant \xi \leqslant t$. In Eq. (A1), R_ξ is the autocorrelation of the transverse component of the flame front velocity (v_f) and is obtained from the following equation [25]:

$$R_\xi = 1 + \sum_{n=1}^{\infty} (-1)^n \frac{\xi^{2n}}{(2n)!} \left[\frac{\left(\frac{\mathrm{d}^n v_f}{\mathrm{d}t^n}\right)|_{t=0}}{v_f} \right]^2. \tag{A2}$$

In Eq. (A2), $\frac{\mathrm{d}^n}{\mathrm{d}t^n}$ is the nth order derivative with respect to time. Estimating Eq. (A2) requires time-resolved measurement of the flame front velocity, which is not performed in the present study. However, as a first approximation, the term pertaining to the transverse component of the flame front velocity in Eq. (A2) can be simplified, and, as a result, R_ξ can be estimated. Specifically, it was assumed that:

$$\frac{\left(\frac{\mathrm{d}^n v_f}{\mathrm{d}t^n}\right)|_{t=0}}{v_f} \approx \frac{\frac{v_f}{\tau^n}}{v_f} = \tau^{-n}, \tag{A3}$$

where τ is a time scale associated with movements of the flame front in the transverse direction. Since the nominator of the left-hand-side of Eq. (A3) is estimated at $t = 0$, τ was also evaluated for this condition. Since ξ varies between 0 and t, for $t = 0$, $\xi = 0$. Eq. (A2) shows that, at $\xi = 0$, $R_\xi = 1$. Argument provided in Taylor [25] show that, for $R_\xi = 1$, the time scale associated with movements of the particles in the transverse direction to the flow, here the time scale associated with movements of the flame front, i.e., τ, approximately equals to y/U. Thus, Eq. (A3) can be simplified into the following equation:

$$\frac{\left(\frac{\mathrm{d}^n v_f}{\mathrm{d}t^n}\right)|_{t=0}}{v_f} \approx \left(\frac{y}{U}\right)^{-n}. \tag{A4}$$

Substituting Eq. (A4) into Eq. (A2) results in:

$$R_\xi \approx 1 + \sum_{n=1}^{\infty} (-1)^n \frac{\xi^{2n}}{(2n)!} (y/U)^{-2n}. \tag{A5}$$

Using Eq. (A5), the double integral in Eq. (A1) was estimated, and Eq (A1) was simplified to:

$$\begin{aligned} x'^2 &\approx v_f'^2 (y/U)^2 \left(1 + 2\sum_{n=1}^{\infty} \frac{(-1)^n}{(2n+2)!}\right) \\ &\approx 2 v_f'^2 (y/U)^2 (1 - \cos(1)). \end{aligned} \tag{A6}$$

Solving Eq. (A6) for the RMS of the transverse component of the flame front velocity results in:

$$v_f' \approx \frac{x' U}{y}. \tag{A7}$$

Appendix B. Effect of flow three-dimensionality on mean of the normal component of edge velocity

All the measurements preformed in the present study are two-dimensional. The three-dimensional nature of the problem can potentially affect statistics of the component of the edge velocity in the normal direction to the flame surface ($\overrightarrow{V_e} \cdot \vec{n}$). The following provides an argument associated with the effect of flow three-dimensionality on the reported values of $\overrightarrow{V_e} \cdot \vec{n}$.

The three-dimensionality of the turbulent premixed flames can potentially result in out-of-plane orientation of the flame surface as well as nonzero values of velocity component in the direction normal to the plane of measurements. Figure 13 shows schematic of a representative flame front in the plane of measurements. In the figure, α is the angle between $\vec{n}$ and the projection of $\vec{n}$ in the plane of measurements. Also shown in the figure are representative unit vector normal to the flame surface ($\vec{n}$) along with the component of the edge velocity normal to the plane of measurements (w_e).

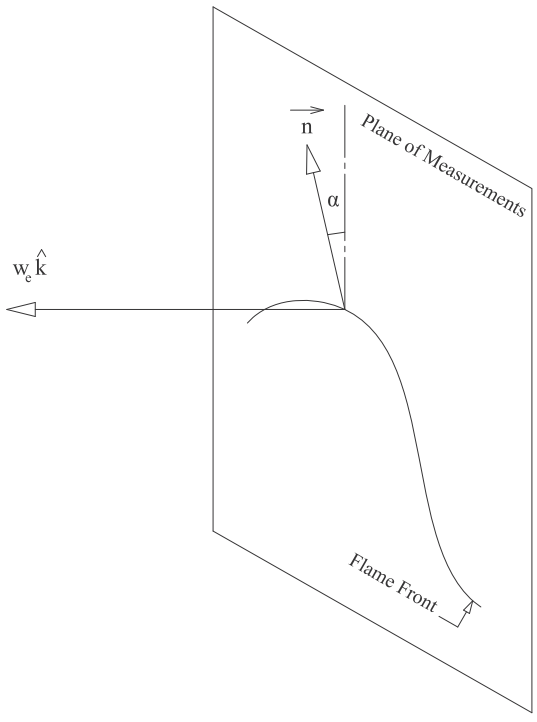

Fig. 13. Schematics of a representative flame front in the plane of measurements.

Knaus et al. [26], Kerl et al. [10], and Chen et al. [27] experimentally measured α for V-shaped flame configuration, stagnation flame, and flame stabilized in a diffuser-type burner, respectively. Their results, show that the out-of-plane orientation of the flame surface is negligible. Specifically, Knaus et al. [26] show that the PDF of α features a delta function at 0°. Thus, $\vec{n}$ remains in the plane of measurements. This means that the flame fronts feature a two-dimensional structure (see pages 118 and 127 in [26]).

The nonzero value of the third component of the velocity data affects two-dimentionaly estimated values of $\overrightarrow{V_e} \cdot \vec{n}$, by addition of the term: $w_e \sin(\alpha)$. Specifically, it can be shown that:

$$\overrightarrow{V_e^{3d}} \cdot \vec{n} = \overrightarrow{V_e} \cdot \vec{n} + w_e \sin(\alpha), \tag{B1}$$

where $\overrightarrow{V_e^{3d}}$ represents values of edge velocity estimated from a three-dimensional measurement. Utilizing the results of Knaus et al. [26], it can be argued that, due to values of α being close to zero, values of $w_e \sin(\alpha)$ are negligible; and, as a result, $\overline{w_e \sin(\alpha)} \approx 0$. This means that $\overline{\overrightarrow{V_e^{3d}} \cdot \vec{n}} \approx \overline{\overrightarrow{V_e} \cdot \vec{n}}$. Analysis of the results presented in Kerl et al. [10] shows a somewhat similar conclusion. Values of $\overline{w_e \sin(\alpha)}$ were extracted from their results. It was obtained that $\overline{w_e \sin(\alpha)} \approx 0.3 S_L \approx 0.1$ m/s. This implies that the contribution of the third component of the edge velocity in $\overline{\overrightarrow{V_e^{3d}} \cdot \vec{n}}$ is not significant.

The conclusion drawn from the studies of Knaus et al. [26] and Kerl et al. [10] shows that the effect of flow three-dimentionality on the mean of the normal component of edge velocity is negligible. Thus, it is belived that the three-dimensional nature of the flow does not significantly affect $\overline{\overrightarrow{V_e} \cdot \vec{n}}$.

Appendix C. Estimation of the mean flame front velocity

Schematics of trajectory of a flamelet center is presented in Fig. 14 by the solid curve. The straight line shown in the figure represents the flamelet. Note that the flamelet orientation is chosen arbitrarily. The hollow symbol in Fig. 14 corresponds to instants at which the center of the flamelet position is known. The position vector of the flamelet center is denoted by $\overrightarrow{x_{f,i}}$ at each circular data symbol. The mean velocity of the flamelet center can be obtained from:

$$\overrightarrow{\overline{V_f}} = \overline{\frac{d\overrightarrow{x_f}}{dt}} \approx \frac{1}{N} \sum_{i=1}^{N-1} \frac{\overrightarrow{x_{f,i+1}} - \overrightarrow{x_{f,i}}}{\Delta t} \approx \frac{\overrightarrow{x_{f,N}} - \overrightarrow{x_{f,1}}}{N \Delta t}, \tag{C1}$$

where N refers to the number of points along the flamelet center trajectory. Assuming that the flamelet is confined within the region

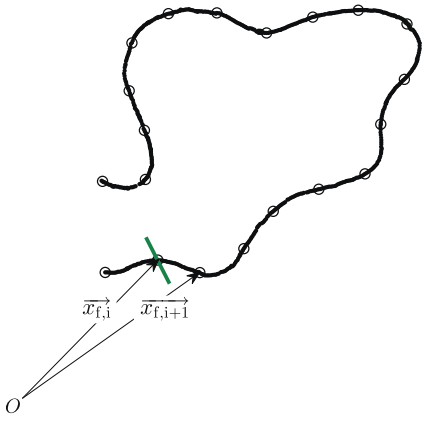

Fig. 14. Representative trajectory of a flamelet.

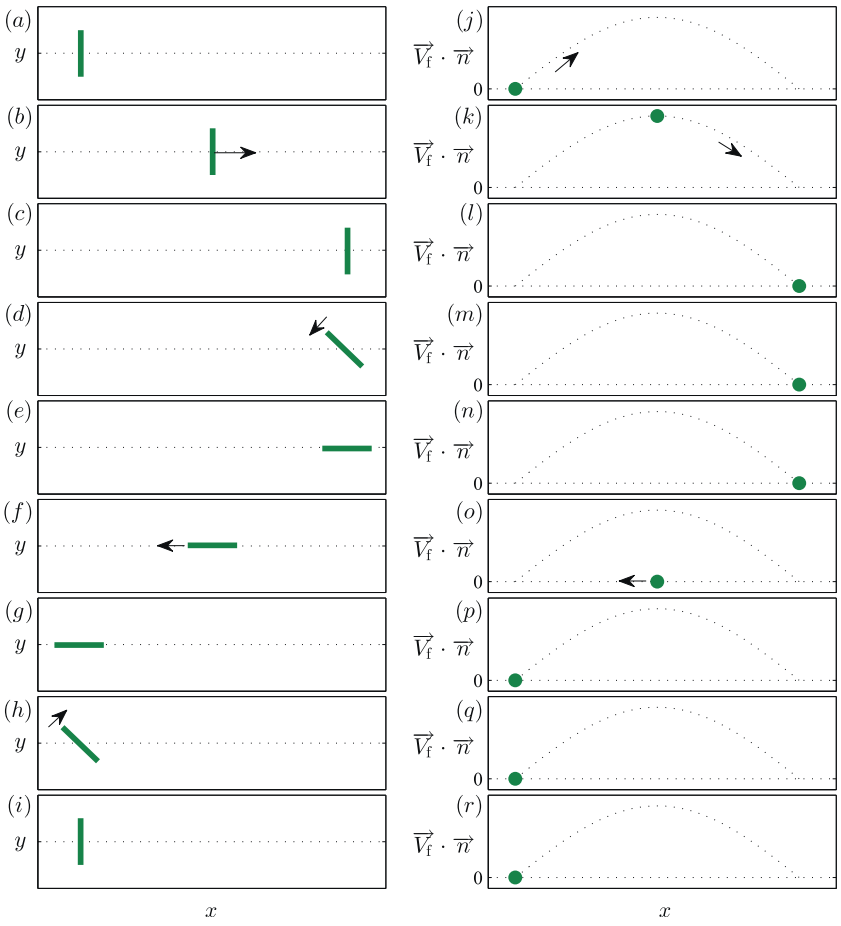

Fig. 15. (a)–(i) Time history of flamelet movement and (j)–(r) time history of the component of the flamelet velocity normal to the flame flamelet.

of measurement, it can be shown that $\overline{\overrightarrow{V_f}}$ is a zero vector if the value of N is selected to be large enough.

It is important to note that the mean of the flamelet velocity being zero does not necessitate the mean of the component of the flamelet velocity in the direction normal to the flamelet is also zero. This is investigated in further details using the following example. Figure 15(a)–(i) present schematics of a flamelet movement. Figure 15(a)–(i) correspond to one complete cycle of movement of the flamelet. Thus, Fig. 15(a) and (i) represent identical positions of the flamelet. The arrows in the figures show the direction of the flamelet movement. Representative values of the component of the flame front velocity in the direction normal to the flamelet is presented in Fig. 15(j)–(r), corresponding to Fig. 15(a)–(i), respectively. As shown in Fig. 15(j)–(r), the component of the flamelet velocity in the direction normal to the flamelet is more than or equal to zero. This means that, in a process that the flamelet movement repeats several times such that $N\Delta t$ is large enough, $\overline{\overrightarrow{V_f}} \cdot \vec{n}$ is nonzero. Thus, mean of the component of the flame front velocity normal to the flame front can attain a nonzero value.

References

[1] N. Peters, Turbulent Combustion, first ed., Cambridge University Press, 2000.
[2] I. Glassman, R.A. Yetter, Combustion, fourth ed., Elsevier Inc., 2008.
[3] P. Clavin, Prog. Energy Combust. Sci. 11 (1985) 1–59.
[4] A.N. Lipatnikov, J. Chomiak, Prog. Energy Combust. Sci. 28 (2002) 1–74.
[5] J.F. Driscoll, Prog. Energy Combust. Sci. 34 (2008) 91–134.
[6] I.G. Shepherd, G.L. Hubbard, L. Talbot, Proc. Combust. Inst. 21 (1986) 1377–1383.
[7] P. Giox, P. Paranthoen, M. Trinité, Combust. Flame 81 (1990) 229–241.
[8] S. Kheirkhah, Ö.L. Gülder, Phys. Fluids 25 (2013) 055107.
[9] B. Renou, A. Boukhalfa, D. Puechberty, M. Trinité, Proc. Combust. Inst. 27 (1998) 841–847.
[10] J. Kerl, C. Lawn, F. Beyrau, Combust. Flame 160 (2013) 2757–2769.
[11] I.R. Gran, T. Echekki, J.H. Chen, Proc. Combust. Inst. 26 (1996) 323–329.
[12] J.H. Chen, H.G. Im, Proc. Combust. Inst. 27 (1998) 819–826.
[13] A.C. Eckbreth, Laser Diagnostics for Combustion Temperature and Species, second ed., Overseas Publishers Association, 1996.
[14] J.B. Bell, M.S. Day, I.G. Shepherd, M.R. Johnson, R.K. Cheng, J.F. Grcar, V.E. Beckner, M.J. Lijewski, Proc. Natl. Acad. Sci. U.S.A. 102 (29) (2005) 10006–10011.
[15] J.R. Hertzberg, M. Namazian, L. Talbot, Combust. Sci. Technol. 38 (1984) 205–216.
[16] D.A. Knaus, F.C. Gouldin, Proc. Combust. Inst. 28 (2000) 367–373.
[17] S.S. Sattler, D.A. Knaus, F.C. Gouldin, Proc. Combust. Inst. 29 (2002) 1785–1792.
[18] N. Peters, Proc. Combust. Inst. 21 (1986) 1231–1250.
[19] P.C. Miles, F.C. Gouldin, Proc. Combust. Inst. 24 (1992) 477–484.
[20] S.B. Pope, Turbulent Flows, first ed., Cambridge University Press, 2000.
[21] G.E. Andrews, D. Bradley, Combust. Flame 19 (1972) 275–288.
[22] J. Jarosinski, Combust. Flame 56 (1984) 337–342.
[23] R.K. Cheng, Combust. Sci. Technol. 41 (1984) 109–142.
[24] K.V. Dandekar, F.C. Gouldin, AIAA J. 20 (5) (1981) 652–659.
[25] I.G. Taylor, Proc. London Math. Soc. 20 (1922) 196–212.
[26] D.A. Knaus, F.C. Gouldin, D.C. Bingham, Assessment of crossed plane tomography for flamelet surface normal measurements, Combust. Sci. Technol. 174 (2002) 101–134.
[27] Y.-C. Chen, M. Kim, J. Han, S. Yun, Y. Yoon, Proc. Combust. Inst. 31 (2007) 1327–1335.